

Jahn-Teller driven perpendicular magnetocrystalline anisotropy in metastable Ru

Dorj Odkhuu^{1,2}, S. H. Rhim^{1,3,*}, Noejung Park⁴, Kohji Nakamura⁵, and Soon-Cheol Hong^{1†}

¹ Department of Physics and Energy Harvest Storage Research Center,
University of Ulsan, Ulsan, Korea

² Department of Physics, Incheon National University,
Incheon, Korea ³ Department of Physics and Astronomy,
Northwestern University, Evanston, IL, 60208

⁴ Department of Physics, UNIST, Ulsan, Korea

⁵ Department of Physics Engineering,
Mie University, Tsu, Mie, 514-8507, Japan

(Dated: September 24, 2018)

A new metastable phase of the body-centered-tetragonal ruthenium (*bct*-Ru) is identified to exhibit a large perpendicular magnetocrystalline anisotropy (PMCA), whose energy, E_{MCA} , is as large as $150 \mu\text{eV/atom}$, two orders of magnitude greater than those of $3d$ magnetic metals. Further investigation over the range of tetragonal distortion suggests that the appearance of the magnetism in the *bct*-Ru is governed by the Jahn-Teller split e_g orbitals. Moreover, from band analysis, MCA is mainly determined by an interplay between two e_g states, $d_{x^2-y^2}$ and d_{z^2} states, as a result of level reversal associated with tetragonal distortion.

PACS numbers: 75.30.Gw, 75.50.Cc, 75.70.Tj

Physics phenomena originated from spin-orbit interaction, such as magneto-crystalline anisotropy (MCA), Rashba-type interactions, or topological insulator, have attracted huge attention for its intriguing physics as well as great potential for spintronics applications.¹⁻⁵ In particular, MCA, where one particular direction of the magnetization is energetically preferred, offers opportunities in spintronics such as magnetic random access memory (MRAM), spin-transfer torque (STT), magneto-optics, and to list a few. With advances of fabrication techniques in recent years, search for materials with large MCA, more preferably perpendicular MCA (PMCA), has been very intensive.

In particular, ferromagnetic films that can provide perpendicular MCA (PMCA) are indispensable constituents in STT memory that utilizes spin-polarized tunneling current to switch magnetization.⁶ For practical operation of high-density memory bits, two criteria have to be satisfied for practical usage of high-density magnetic storage - low switching current (I_{SW}) and thermal stability. Small volume is favored to lower I_{SW} , but is detrimental for the thermal stability. However, the shortcoming of small volume can be compensated by large MCA while still retaining the thermal stability. On the other hand, low magnetization will offer advantage to reduce stray field in real devices. Therefore, exploration for materials with high anisotropy and small magnetization would be one favorable direction to minimize I_{SW} and at the same time to maximize the thermal stability.

In the framework of perturbation theory⁷, E_{MCA} is determined by the spin-orbit interaction between occupied and unoccupied states as,

$$E_{MCA}^{\sigma\sigma'} \approx \xi^2 \sum_{o,u} \frac{|\langle o^\sigma | \ell_z | u^{\sigma'} \rangle|^2 - |\langle o^\sigma | \ell_x | u^{\sigma'} \rangle|^2}{\epsilon_{u,\sigma'} - \epsilon_{o,\sigma}}, \quad (1)$$

where o^σ ($u^{\sigma'}$) and $\epsilon_{o,\sigma}$ ($\epsilon_{u,\sigma'}$) represent eigenstates and eigenvalues of occupied (unoccupied) for each spin state, $\sigma, \sigma' = \uparrow, \downarrow$, respectively; ξ is the strength of spin-orbit coupling (SOC).

As the electronic structure of magnetic materials with non-negligible MCA is mainly dominated by d electrons, it would be worthwhile to see how energy levels of d orbitals evolve in different crystal symmetry, as illustrated in Fig. 1. For the *bcc*-Ru with $c/a = 1$, the cubic symmetry splits five d orbitals into doublet (e_g) and triplet (t_{2g}). When the lattice changes from high-symmetric body-centered to tetragonal with lower symmetry, additional Jahn-Teller splitting may offer more freedom to provide more energy differences in Eq. (1). More specifically, d electrons in the *bcc* structure split into doublet (e_g) and triplet (t_{2g}). The tetragonal distortion further splits these e_g and t_{2g} levels into two irreducible representations: e_g into two singlets a_1 (d_{z^2}) and b_1 ($d_{x^2-y^2}$); t_{2g} into a singlet b_2 (d_{xy}) and a doublet e ($d_{yz,xz}$), where their relative order is determined by c/a , either larger or smaller than unity.

Metals with $4d$ and $5d$ valence electrons possess inherently larger SOC than conventional $3d$ metals. Search for magnetism in these transition metals have a long history. The fact that Pd and Pt barely miss the Stoner criteria to become ferromagnetic (FM) has incurred enormous efforts to realize magnetism in several multilayers and interfaces of $4d$ metals by adjusting volumes or lattice constants, thereby increased density of states (DOS) at the Fermi level (E_F), $N(E_F)$, due to narrowed bandwidth, would meet the Stoner criteria. Hence, $4d$ and $5d$ metals with large SOC as well as magnetism would be favorable candidate to realize large MCA.

Previous theoretical study suggested that ferromagnetism in Ru is feasible in body-centered-cubic (*bcc*) structure when lattice is expanded by 5%.⁸ Other studies predicted that magnetism can occur in Rh and Pd with volume changes.^{9,10} However, those theoretically proposed magnetism associated with volume changes in $4d$ metals have not been fully confirmed experimentally. Nevertheless, with remarkable advances in recent fabrication techniques, various types of lattices are now accessible with diverse choice of substrates. In particular, the *bct*-Ru film has been successfully fabricated on the Mo (110) substrate, whose lattice constants are $a=3.24 \text{ \AA}$ and $c/a=0.83$

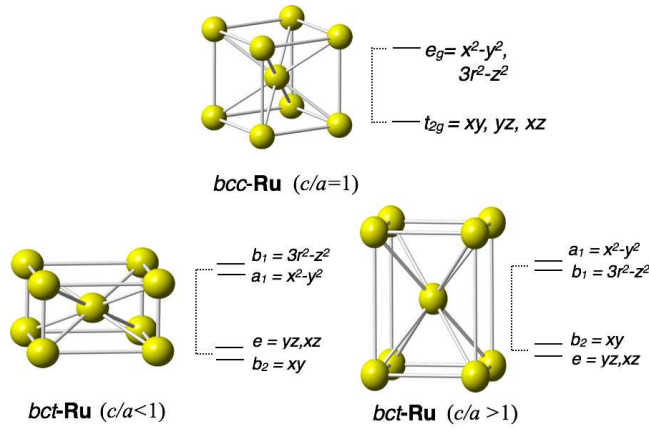


FIG. 1: (color online) Schematic presentation of the Jahn-Teller splitting of d electrons. In the cubic symmetry, such as bcc ($c/a = 1$), d orbital splits into doublet (e_g) and triplet (t_{2g}). Tetragonal distortion further splits e_g into a_1 and b_1 ; t_{2g} into a singlet b_2 and a doublet e , where their relative order is shown depending on c/a is greater or smaller than unity.

as identified by X-ray electron diffraction.¹¹ Later, theoretical calculation argued that magnetism can exist in the bct -Ru for $c/a = 0.84$ with moment of $0.4 \mu_B/\text{atom}$.¹²

In this paper, we present that in a newly identified metastable phase of the bct -Ru, E_{MCA} can be as large as $150 \mu\text{eV}/\text{atom}$, two orders of magnitude greater than those in $3d$ magnetic metals. The magnetic instability driven by this tetragonal distortion is discussed in connection with the Stoner criteria. Furthermore, we show that magnetism as well as MCA are governed mainly by the Jahn-Teller split e_g orbitals.

Density functional calculations were performed using the highly precise full-potential linearized augmented plane wave (FLAPW) method.¹³ For the exchange–correlation potential, generalized gradient approximation (GGA) was employed as parametrized by Perdew, Burke and Ernzerhof (PBE).¹⁴ Energy cutoffs of 16 and 256 Ry were used for wave function expansions and potential representations. Charge densities and potential inside muffin-tin (MT) spheres were expanded with lattice harmonics $\ell \leq 8$ with MT radius of 2.4 a.u. To obtain reliable values of MCA energy (E_{MCA}), calculations with high precision is indispensable. A $40 \times 40 \times 40$ mesh in the irreducible Brillouin zone wedge is used for k point summation. A self-consistent criteria of $1.0 \times 10^{-5} e/(a.u.)^3$ was imposed for calculations, where convergence with respect to the numbers of basis functions and k points was also seriously checked.^{15,16} For the calculation of E_{MCA} , torque method^{7,17} was employed to reduce computational costs, whose validity and accuracy have been proved in conventional FM materials.^{18–23}

Equilibrium lattice constants of hexagonal-closed-packed (hcp)-, face-center-cubic (fcc)-, and bcc -Ru are summarized in Table I, which are in good agreement with experiments,^{11,24} and previous work.¹² The hcp structure is the most stable phase, as Ru crystallizes in hcp . However, the energy difference between hcp and fcc , $0.07 \text{ eV}/\text{atom}$, is very small, which reflects the feature of closed packed structures of the two but with different stacking sequences. In Fig. 2(a) total energy

of non-magnetic (NM) bct -Ru as a function of tetragonal distortion (c/a) is plotted for the fixed volume of the equilibrium bcc -structure. Our result reproduces that by Watanabe *et al.*¹²: There is a global minimum at $c/a = 1.41$ corresponding to the fcc structure. There are two other extrema, a local maximum and minimum at $c/a = 1$ and $c/a = 0.84$, respectively. In particular, the local minimum at $c/a = 0.84$ suggests the exist-

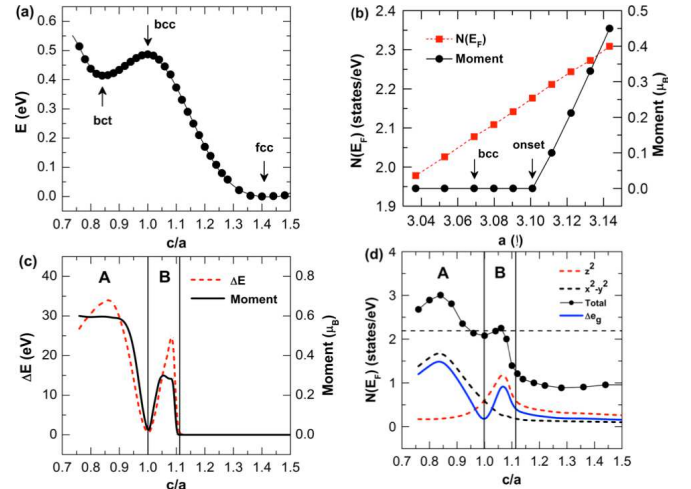


FIG. 2: (color online) (a) Total energy with respect to fcc structure ($c/a=1.41$) of non-magnetic bct -Ru upon the tetragonal distortion (c/a) in fixed volume of the bcc structure. The equilibrium c/a for bct , bcc , and fcc are denoted. (b) $N(E_F)$ of non-spin-polarized calculations (red squares), and magnetic moment of the bcc -Ru as a function of the uniform lattice constant a (black circles). The arrow denotes the equilibrium lattice constant of bcc -Ru. (c) Energy difference $\Delta E = E_{NM} - E_{FM}$ (red dotted line), magnetic moments (black solid line) as function of c/a . The tetragonal distortion is classified into two regions, A and B, by $c/a < 1$ or > 1 . (d) $N(E_F)$ of NM bct -Ru as function of c/a . Total $N(E_F)$, those from d_{z^2} , $d_{x^2-y^2}$, and the absolute value of the difference of the two e_g orbitals, denoted as Δe_g , are shown in black solid circles, black dotted line, red dashed line, and blue solid line, respectively.

TABLE I: Calculated equilibrium lattice parameters, a and c/a (in Å), and total energy difference ΔE (in eV/atom) of hcp -, fcc -, bcc -, and bct -Ru with respect to the total energy of hcp structure. Experimental and previous theoretical results are also given for comparison.

	hcp		fcc		bcc		bct		
	Present	Experiment ^a	Present	Previous ^b	Present	Previous	Present	Previous ^b	Experiment ^a
a	2.70	2.70	3.84	3.84	3.07	3.06	3.25	3.25	3.24
c/a	1.58	1.58	1.09	1.00	1.00	1.00	0.84	0.83	0.83
ΔE	0.0		0.07	0.13	0.56	0.65	0.48	0.55	-

^aShiiki *et al.*¹¹

^bWatanabe *et al.*¹²

tence of metastable phase as discussed in Ref.¹². Further calculations of total energy of the bct structure as function of both a and c/a confirms that the local minimum is at $a = 3.25$ Å and $c/a = 0.84$, consistent with the fixed volume calculation of the bcc structure.

In Fig. 2(b), $N(E_F)$ of non-spin-polarized and magnetic moment of spin-polarized calculation are plotted as function of lattice constant. The onset of magnetism in the bcc phase occurs at $a = 3.10$ Å, which corresponds to 1.1% expansion of lattice constant, or 3.3% expansion of volume, as consistent with Ref.⁸. In order for the magnetic instability in the bcc phase to satisfy the Stoner criteria, $I \cdot N(E_F) \geq 1$, and from the fact that the Stoner factor I of a particular atom does not differ substantially in different crystal structures, we estimate $I = 0.46$ eV for Ru from $N(E_F) = 2.18$ eV⁻¹.

On the other hand, as shown in Fig. 2(c), the energy difference between NM and FM states ($\Delta E = E_{NM} - E_{FM}$) and magnetic moment reveal almost the same trends as c/a changes. ΔE of the bcc - and fcc -phases are negligibly small, thus both phases are non-magnetic. When $c/a < 1.1$ but $c/a \neq 1$, the bct -Ru is magnetic ($\Delta E > 0$), whereas $c/a > 1.1$, it is non-magnetic. In particular, $c/a = 0.84$ gives $\Delta E = 35$ meV/atom with magnetic moment as high as $0.6 \mu_B$, larger than $0.40 \mu_B$ by Ref.¹². Interestingly, the magnetic moment of the bct -Ru exhibits a re-entrance behavior for $c/a > 1$, as predicted by Schönecker *et al.*²⁵. In region A ($c/a < 1$), magnetic moment decreases as c/a increases, whereas magnetism reappears when c/a just passes unity, which eventually vanishes for $c/a > 1.1$.

Total DOS and those from e_g orbitals at E_F as function of c/a are plotted in Fig. 2(d) for the NM bct -Ru. Most contributions come from the Jahn-Teller split e_g orbitals, whose difference in DOS is also plotted: It resembles magnetic moment shown in Fig. 2(c). Moreover, among the Jahn-Teller split e_g orbitals, $d_{x^2-y^2}$ (d_{z^2}) dominates the other for $c/a < 1$ ($c/a > 1$).

Partial DOS (PDOS) of d orbitals are shown in Fig. 3 for the spin-polarized cases, where the trivial $c/a = 1$ is omitted. Prominent peaks at $c/a = 0.84$ are mainly from $d_{x^2-y^2}$ states with occupied (unoccupied) peaks in majority (minority) spin bands, while peaks in d_{z^2} states evolve as c/a increases. Contributions from t_{2g} states are rather featureless.

For simplicity, we assign the energy difference of peaks in e_g states, $d_{x^2-y^2}$ for $c/a < 1$ and d_{z^2} for $c/a > 1$, respectively, as the exchange-splitting. Then, as c/a increases, the exchange-splittings are 1.02, 1.05, 0.80, and 0.66 eV for

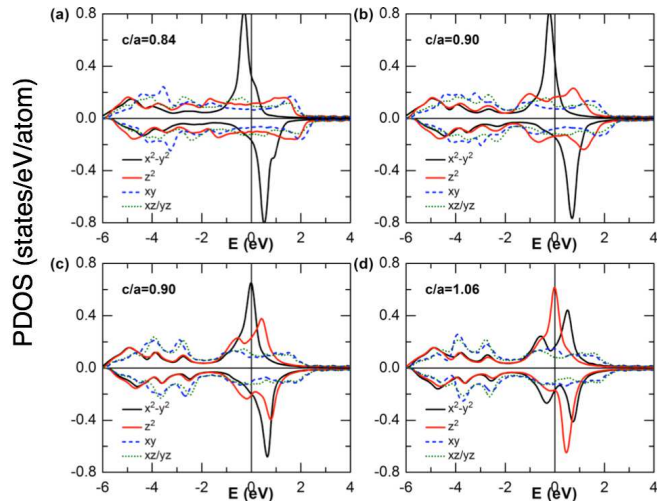


FIG. 3: (color online) Orbital-decomposed DOS of d -orbital for spin-polarized calculations of bct -Ru at $c/a =$ (a) 0.84, (b) 0.90, (c) 0.96, and (d) 1.06, respectively. The d orbital states are shown in different colors: red (d_{z^2}), black ($d_{x^2-y^2}$), blue (d_{xy}), and green ($d_{xz,yz}$), respectively.

$c/a = 0.84, 0.90, 0.96,$ and 1.06 , respectively, which qualitatively reflects magnetism of the bct -Ru. From this, the exchange-splitting is mainly determined by one of the Jahn-Teller split e_g orbitals.

In addition to magnetism, the bct -Ru exhibits large MCA. The angle-dependent total energy in a tetragonal symmetry is expressed in the most general form, $E_{tot}(\theta, \varphi) = E_0 + k_1 \sin^2 \theta + k_2 \sin^4 \theta + k_3 \sin^4 \theta \cos 4\varphi$, where θ and φ are polar and azimuthal angles, respectively, and $k_1 = 100$, $k_2 = -1$, and $k_3 \ll 1$ μeV . The small value of k_3 indicates negligible φ dependence. $E_{MCA} = E_{tot}(\theta = 90^\circ) - E_{tot}(\theta = 0^\circ)$ as function of the tetragonal distortion c/a is shown in Fig. 4(a). $E_{MCA} = 150$ $\mu\text{eV}/\text{atom}$ at $c/a = 0.80$, and $E_{MCA} = 100$ $\mu\text{eV}/\text{atom}$ for the local minimum ($c/a = 0.84$), which are two orders of magnitude greater than conventional $3d$ magnetic metals. As the strength of the tetragonal distortion changes, E_{MCA} changes not only in magnitude but also in sign. In region A, E_{MCA} becomes negative near $c/a \approx 0.9$ and reaches -100 $\mu\text{eV}/\text{atom}$ around $c/a = 0.96$, whereas in region B, $E_{MCA} > 0$: PMCA is restored. Hence, the strength of the tetragonal distortion, c/a , influences magnetic moments as well as E_{MCA} .

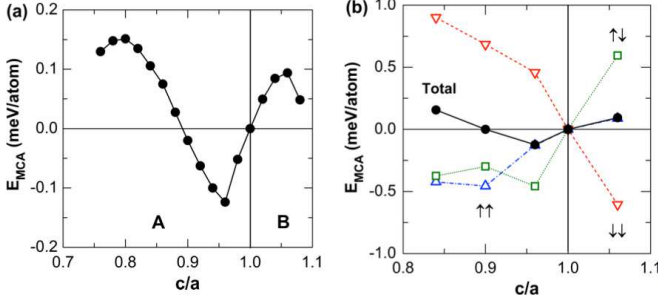


FIG. 4: (color online) (a) MCA energy dependence on c/a for bct -Ru, where AB are defined as in Fig. 2(b). (b) Spin-channel decomposed and total E_{MCA} of bct -Ru for various c/a . Black circles denote total MCA. Upper (lower) triangles denote $\uparrow\uparrow$ ($\downarrow\downarrow$)-channel, squares denote $\uparrow\downarrow$ -channel.

E_{MCA} is decomposed into different spin-channels following Eq. (1), as shown in Fig. 4(b) for the bct -Ru with $c/a=0.84, 0.90, 0.96$ and 1.06 , respectively. For $\sigma\sigma'=\uparrow\uparrow$ or $\downarrow\downarrow$, positive (negative) contribution to E_{MCA} is determined by the SOC interaction between occupied and unoccupied states with the same (different by one) magnetic quantum number (m) through the ℓ_Z (ℓ_X) operator. For $\sigma\sigma'=\uparrow\downarrow$, Eq. (1) has opposite sign, so positive (negative) contribution come from the ℓ_X (ℓ_Z) coupling.

From the spin-channel decomposition of E_{MCA} , one notes that there is no dominant spin-channel. This feature differs from the $3d$ transition metals, where particular spin-channel, i.e. the $\downarrow\downarrow$ -channel, dominantly contributes to positive value through the SOC matrix $\langle x^2 - y^2 | \ell_Z | xy \rangle$ with negligible ones from ℓ_X matrices.^{7,26} When $c/a=0.84$, the $\downarrow\downarrow$ -channel gives the largest contribution, while those from other channels are smaller than half of the $\downarrow\downarrow$ -channel with opposite signs. As c/a increases, the $\downarrow\downarrow$ -channel contribution is reduced, which turns negative for $c/a > 1$. MCA almost vanishes for $c/a=0.90$ and becomes negative for $c/a=0.96$. On the other hand, for $c/a=1.06$, the $\uparrow\downarrow$ - and $\downarrow\downarrow$ -channels contribute almost the same magnitudes with opposite signs, so just the $\uparrow\uparrow$ -channel contribution remains.

To obtain more insights, band structure is plotted in Fig. 5 with d orbital projection, where size of symbols is proportional to their weights. All bands along the Γ -Z are highly dispersive, whereas those along the X -P- N - Γ -X are less dispersive with rather flat feature from $d_{x^2-y^2}$ and d_{z^2} states. Level reversals between e_g states, $d_{x^2-y^2}$ and d_{z^2} , are well manifested, while t_{2g} states are relatively rigid with respect to tetragonal distortion. It is a formidable task to identify the role of each individual SOC matrix for each c/a . However, from the spin-channel decomposed MCA [Fig. 4(b)], each spin-channel changes its sign when c/a becomes greater than unity, where the level reversal occurs between $d_{x^2-y^2}$ and d_{z^2} .

For a simple analysis, we express the $\downarrow\downarrow$ -channel as

$$E(\downarrow\downarrow) = \frac{|\langle x^2 - y^2 | \ell_Z | xy \rangle|^2}{\epsilon_{x^2-y^2} - \epsilon_{xy}} - \frac{|\langle x^2 - y^2 | \ell_X | xz \rangle|^2}{\epsilon_{x^2-y^2} - \epsilon_{xz}} - \frac{|\langle z^2 | \ell_X | xz \rangle|^2}{\epsilon_{z^2} - \epsilon_{xz}}. \quad (2)$$

We focus along the X -P- N - Γ -X, where e_g are unoccupied.

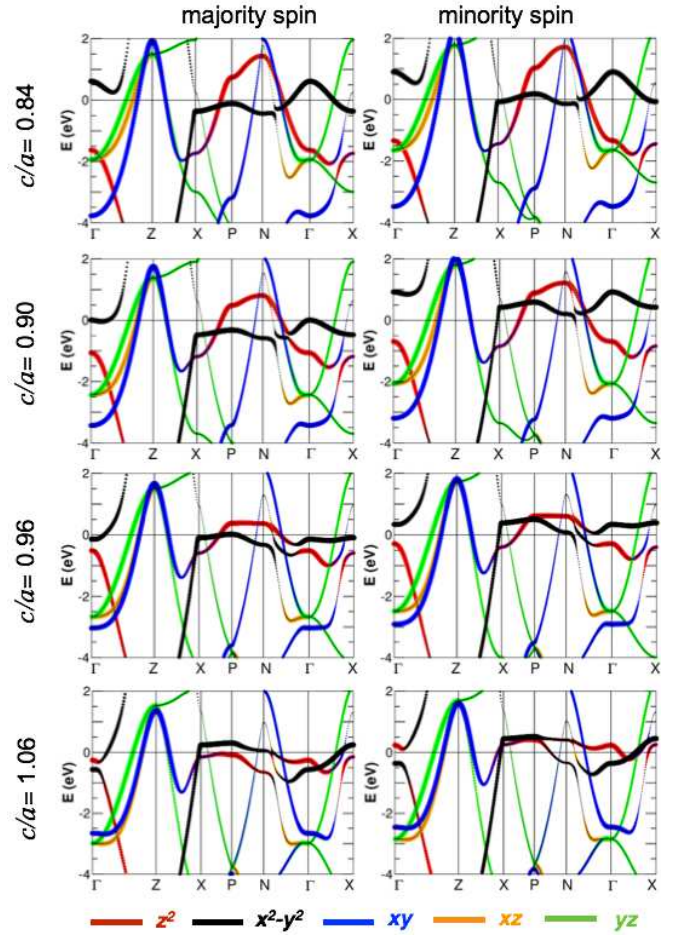


FIG. 5: (color online) Band structures of bct -Ru for $c/a=0.84, 0.90, 0.96$, and 1.06 for majority and minority spin states. d orbital states are shown in different colors: red (d_{z^2}), black ($d_{x^2-y^2}$), blue (d_{xy}), orange (d_{xz}), and green (d_{yz}), respectively.

The $\langle yz | \ell_Z | xz \rangle$ contributions are neglected due to the rigidity of t_{2g} states as well as their small contribution to E_{MCA} owing to large energy denominator. From the fact that $E(\downarrow\downarrow) > 0$ when $c/a=0.84$ with the largest value, we can infer that the first term in Eq. (2) should be larger than the other two, where the largest occur along the P- N . [See Supplementary Information (SI) for the k -resolved MCA analysis.]

As c/a increases but $c/a < 1$, the empty d_{z^2} band moves downward while the empty $d_{x^2-y^2}$ band goes upward with respect to E_F . As a result, the third term is enhanced due to smaller energy denominator. Hence, $E(\downarrow\downarrow)$ decreases but remains positive. When $c/a > 1$, however, the level reversal between e_g states pushes d_{z^2} above E_F and $d_{x^2-y^2}$ below E_F along the N - Γ -X. The former provides additional negative contribution while the latter reduces positive contribution. As a consequence, $E(\downarrow\downarrow) < 0$ for $c/a > 1$. The sign behavior of the $\uparrow\downarrow$ -component, $E(\uparrow\downarrow)$, is completely opposite to $E(\downarrow\downarrow)$, as all terms in Eq. (2) take opposite signs.⁷ For the $\uparrow\uparrow$ -component when $c/a < 1$, we focus near the P- N . The largest positive contribution in the $\downarrow\downarrow$ -component is significantly reduced in the $\uparrow\uparrow$ -channel because the empty $d_{x^2-y^2}$ band in the minority

spin is occupied in the majority spin, and the empty d_{z^2} band contributes negatively. Thus, $E(\uparrow\uparrow) < 0$. When $c/a > 1$, the occupancy of e_g states are reversed again due to the level reversal, therefore $E(\uparrow\uparrow) > 0$. We want to point out that the level reversal between the $d_{x^2-y^2}$ and the d_{z^2} states not only affects the sign behavior of MCA but also the exchange-splitting in DOS. Above argument of the sign behavior is more clearly supported by the k -resolved MCA analysis. [See SI Fig. S1-S5.]

In summary, a new metastable phase of the bct -Ru has been identified to exhibit a large PMCA, two orders of magnitude greater than conventional magnetic metals. In the context of spintronics application, this large anisotropy along with low magnetization and small volume would be key factors to realize materials with low switching current and high thermal stability. Magnetism of the bct -Ru is mainly governed by the Jahn-Teller split e_g states. As the strength of the tetragonal distortion changes, magnetism of the bct -Ru shows an inter-

esting reentrance behavior for $1 < c/a < 1.1$. The tetragonal distortion accompanies MCA changes in both magnitudes and signs, as a result of the level reversal between $d_{x^2-y^2}$ and d_{z^2} .

Acknowledgments

DO, SHR, and SCH are supported by Basic Research Program (20100008842) and Priority Research Centers Program (20090093818) through the National Research Foundation (NRF) funded by the Korean Ministry of Education, Science and Technology. NP was supported by Basic Science Research Program through the NRF funded by the Korean Ministry of Education (2013R1A1A2007910). KN acknowledges support from a Grant-in-Aid for Scientific Research (No. 24540344) from the Japan Society for the Promotion of Science. DO and SHR equally contributed authors.

-
- * Email address: sonny@ulsan.ac.kr
 † Email address: schong@ulsan.ac.kr
- ¹ M. Z. Hasan and C. L. Kane, *Rev. Mod. Phys.* **82**, 3045 (2010).
 - ² X.-L. Qi and S.-C. Zhang, *Rev. Mod. Phys.* **83**, 1057 (2011).
 - ³ S. Wolf, D. Aschwalom, R. Buhrman, J. Daughton, S. von Molnár, M. Roukes, A. Y. Chtchelkanova, and D. Tregor, *Science* **294**, 1488 (2001).
 - ⁴ I. Žutić, J. Fabian, and S. das Sarma, *Rev. Mod. Phys.* **76**, 323 (2004).
 - ⁵ A. Brataas, A. D. Kent, and H. Ohno, *Nat. Mater.* **11**, 372 (2012).
 - ⁶ J. Z. Sun, *Phys. Rev. B* **62**, 570 (2000).
 - ⁷ D. S. Wang, R. Q. Wu, and A. J. Freeman, *Phys. Rev. B* **47**, 14932 (1993).
 - ⁸ M. Kobayashi, T. Kai, N. Takano, and K. Shiiki, *J. Phys.: Condens. Matter* **7**, 923 (1994).
 - ⁹ V. L. Moruzzi and P. M. Marcus, *Phys. Rev. B* **39**, 471 (1989).
 - ¹⁰ H. Chen, N. E. Brener, and J. Callaway, *Phys. Rev. B* **40**, 1443 (1989).
 - ¹¹ K. Shiiki and O. Hio, *Jpn. J. Appl. Phys.* **36**, 7360 (1997).
 - ¹² S. Watanabe, T. Komine, T. Kai, and K. Shiiki, *J. Magn. Magn. Mater.* **220**, 277 (2000).
 - ¹³ E. Wimmer, H. Krakauer, M. Weinert, and A. J. Freeman, *Phys. Rev. B* **24**, 864 (1981).
 - ¹⁴ J. P. Perdew, K. Burke, and M. Ernzerhof, *Phys. Rev. Lett.* **77**, 3865 (1996).
 - ¹⁵ Y. Mokrousov, G. Bihlmayer, S. Heinze, and S. Blügel, *Phys. Rev. Lett.* **96**, 147201 (2006).
 - ¹⁶ S. C. Hong and J. I. Lee, *J. Kor. Phys. Soc.* **52**, 1099 (2008).
 - ¹⁷ X. Wang, R. Wu, D.-S. Wang, and A. J. Freeman, *Phys. Rev. B* **54**, 61 (1996).
 - ¹⁸ R. Q. Wu and A. J. Freeman, *J. Magn. Magn. Mater.* **200**, 498 (1999).
 - ¹⁹ D. Odkhuu and S. C. Hong, *J. Appl. Phys.* **107**, 09A945 (2010).
 - ²⁰ Y. N. Zhang and R. Q. Wu, *Phys. Rev. B* **82**, 224415 (2010).
 - ²¹ D. Odkhuu, W. S. Yun, S. H. Rhim, and S. C. Hong, *Appl. Phys. Lett.* **98**, 152502 (2011).
 - ²² D. Odkhuu, W. S. Yun, and S. C. Hong, *J. Appl. Phys.* **111**, 063911 (2012).
 - ²³ D. Odkhuu, S. H. Rhim, N. Park, and S. Hong, *Phys. Rev. B* **88**, 184405 (2013).
 - ²⁴ D. R. Lide, *Handbook of Chemistry and Physics: A Ready Reference Book of Chemical and Physical Data*, 83rd ed. (CRC, New York, 2002).
 - ²⁵ S. Schönecker, M. Richter, K. Koepf, and H. Eschrig, *Phys. Rev. B* **85**, 024407 (2012).
 - ²⁶ K. Hotta, K. Nakamura, T. Akiyama, T. Ito, T. Oguchi, and A. J. Freeman, *Phys. Rev. Lett.* **110**, 267206 (2013).